STRUCTURAL CONTROL AND HEALTH MONITORING
Struct. Control Health Monit. 2006; **13**:758–774
Published online 9 November 2005 in Wiley InterScience (www.interscience.wiley.com). DOI: 10.1002/stc.110

Cubic control for phase I smart base-isolated benchmark building with emphasis on nonstructural performance

Xin Xu[1], Tarunraj Singh[2] and Gary F. Dargush[1,*,†]

[1] *Department of Civil, Structural and Environmental Engineering, SUNY Buffalo, NY 14260, U.S.A.*
[2] *Department of Mechanical and Aerospace Engineering, SUNY Buffalo, NY 14260, U.S.A.*

SUMMARY

Most control techniques in the structural engineering literature are aimed at improving performance of the primary structural system, but may have limited or even adverse effect on nonstructural components during strong seismic events. In this paper, we emphasize nonstructural performance using an active controller with a cubic nonlinearity. The controller is optimized based on the frequency response functions of a SDOF nonlinear oscillator. An eight-storey base-isolated benchmark building recently proposed by the ASCE structural control committee is studied as a demonstration by considering both structural and nonstructural performance indices. We compare the performance of the proposed cubic controller with that of a LQG-based semiactive control system and a passive energy dissipation system. It is shown from the simulation results that in most benchmark test cases, the cubic control system produces better nonstructural performance while maintaining good response characteristics of the primary structural system. Further research directions for this cubic control system are also pointed out. Copyright © 2005 John Wiley & Sons, Ltd.

KEY WORDS: nonstructural components; base-isolated building; cubic control; frequency response function; semi-active trace algorithm; near-fault earthquake

1. INTRODUCTION

It is apparent, as demonstrated in the literature on the subject [1], that the engineering profession has now recognized the importance of seismic design of electrical and mechanical equipment, pipelines, parapets, elevators, tanks, and other nonstructural elements that are usually attached to the walls and floors of large multistory buildings, nuclear power plants, industrial facilities, and offshore platforms. More importantly, it also has been recognized that after the occurrence of a strong earthquake the survival of these so-called secondary systems may be vital to provide emergency services, as is the case for equipment in power stations,

*Correspondence to: Professor Gary F. Dargush, Department of Civil, Structural and Environmental Engineering, SUNY Buffalo, NY 14260, U.S.A.
† E-mail: gdargush@eng.buffalo.edu

Contract/grant sponsor: US National Science Foundation; contract/grant number: EEC-9701471

Received 21 December 2004
Revised 1 April 2005
Accepted 28 May 2005

hospitals, or communication facilities. At present, the most accepted performance indices concerning nonstructural components attached to buildings are the peak and root-mean-square (RMS) absolute floor accelerations.

Base isolation, the most mature structural control technique, has been used widely to protect these critical facilities. But certain severe seismic events, such as some near-fault earthquakes dominated by high-frequency ground acceleration, will increase the isolation deformation, and also increase the superstructure absolute accelerations that are vital to the nonstructural seismic performance. Passive control devices, such as viscous dampers [2], may be used to augment damping at the isolation level to reduce the isolation deformation, but heavy damping may increase superstructure accelerations and drifts [3,4]. Other optimal control systems, developed mainly in automatic control engineering, have been recently introduced to the structural engineering profession, such as the linear quadratic Gaussian (LQG), clipped-optimal and skyhook semiactive control using MagnetoRheological (MR) fluid dampers [5–11]. The control effects of a base-isolated benchmark building employing these active/semi-active control systems are studied and compared in [12–14]. The results show that, while all of these control systems can suppress structural vibration, none can significantly reduce the floor acceleration demands and some systems may even have an adverse effect on the nonstructural performance. It should be also noticed that LQG is a linear, full-state feedback control law, while the clipped-optimal and skyhook algorithms are heuristic nonlinear output feedback schemes.

A very flexible structure, such as a base-isolated building, has some unique characteristics for which the single-degree-of-freedom (SDOF) nonlinear oscillation theory [15,16] can apply. The natural vibration frequency of the 'isolation mode' can be shown to be much lower than those of the 'structural modes' [17], thus the dynamics of a flexible MDOF base-isolated building can be well estimated by a simpler analysis treating the superstructure as rigid. Although the demonstration building is a three-dimensional model [14], we can still approximately treat it as a SDOF oscillator in each of the x- and y-directions when designing the controller. In addition, the main advantage of base isolation is already to reduce the linear stiffness from the fixed-base structure significantly, so it seems appropriate to add weak nonlinearities for control of linear base-isolated structures as a 'fine adjustment' mechanism.

Some researchers [18,19] also studied the nonlinear full-state feedback control for a MDOF model derived from a higher-order cost functional using variational calculus. But the input disturbance information, such as near-fault earthquakes, was neglected in their derivation. Also, the stability and state estimation problems are difficult to address thoroughly. In this paper, we adopt a frequency domain approach to design the nonlinear feedback controller optimized based on the frequency response functions of a SDOF nonlinear oscillator including algebraic cubic stiffness and cubic damping. We add these cubic terms in the controller intentionally as the feedback without changing any linear properties of the original linear isolation system. It is worth noting that the contribution of these cubic terms must be small enough to produce only 'slowly time varying' nonlinear oscillation under harmonic ground excitations. This method represents an extension of the linear oscillation theory that is commonly used by structural engineers today.

The paper opens with a derivation of the frequency response functions of a SDOF nonlinear oscillator in the next section, which leads to the determination of an active controller that includes cubic stiffness and damping. This is followed in Section 3 by a review of the algorithm to trace the control profile of any active controller, using semiactive viscous fluid dampers. This

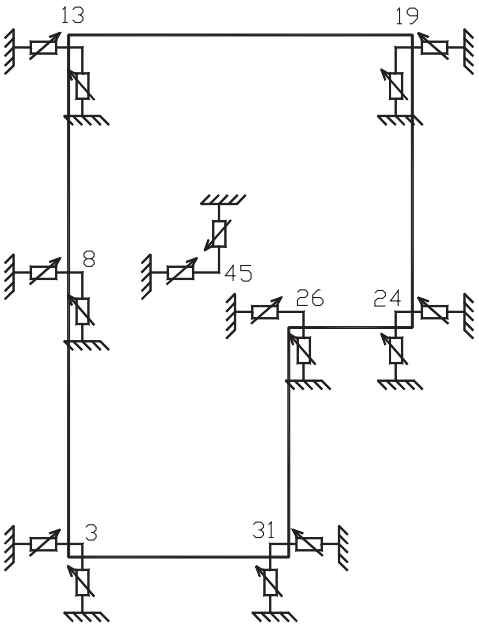

Figure 1. Isolation and control device plan detail.

in conjunction with the generation of results for a passive system, provides us a means to compare the performance of the proposed cubic controller. All the candidate systems are tested on the benchmark structure whose plan is illustrated in Figure 1 where the numbers (3, 8, 13, 19, 24, 26, 31 and 45) correspond to the location of the bearings in the original benchmark problem [14]. Details concerning sensor selection are presented in Section 4, while all simulation results and comparisons are provided in Section 5. The main body of the paper then ends with a number of conclusions in Section 6. An Appendix is also included to clearly define the evaluation criteria for the demonstration problem [14] to be self-contained.

2. DESIGN OF THE CUBIC NONLINEAR CONTROLLER (CUBIC)

The frequency response functions (FRFs) for the relative displacement amplitude and the absolute acceleration amplitude of a SDOF linear oscillator under harmonic ground excitations, are plotted as the curves in Figure 2 versus the normalized frequency ω/ω_1, where ω represents the frequency of the input ground excitation and ω_1 represents the natural frequency of the oscillator.

Notice that heavy linear damping can significantly reduce the steady-state response near the resonant frequency. However, this damping also increases the absolute acceleration throughout the high frequency range of the input ($\omega/\omega_1 > 1.4$). Thus, when a base-isolated building having a low first natural frequency undergoes a strong ground motion containing high frequency contents (> 1 Hz), the acceleration performance may be poor if it is heavily damped. To overcome this dilemma, we introduce algebraic cubic damping and stiffness terms in the

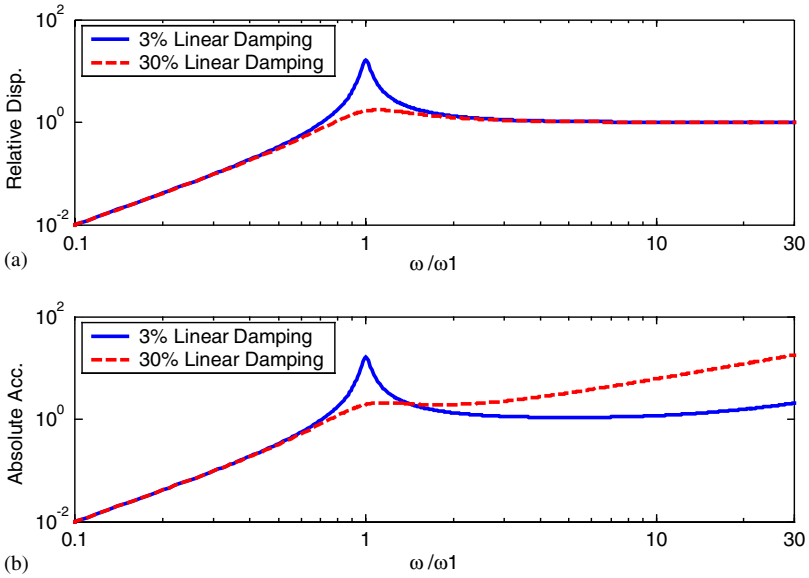

Figure 2. (a) FRFs for the normalized relative displacement of ground-excited linear oscillators with different damping ratios; and (b) FRFs for the absolute acceleration of linear oscillators with different damping ratios.

equation of motion of the uncontrolled isolation system to augment the linear damping and linear stiffness properties. Thus we are considering the following SDOF nonlinear oscillator (Cubic) under a specified harmonic ground excitation:

$$m\ddot{x} + g(z, \dot{z}) = 0 \tag{1}$$

where $g(z, \dot{z}) = C + K$, $C(\dot{z}) = c_3\dot{z}^3 + c_1\dot{z}$, $K(z) = k_3 z^3 + k_1 z$, $x =$ absolute displacement of the oscillator, $z =$ relative displacement of the oscillator with respect to the ground, $k_1 =$ linear stiffness parameter, $c_1 =$ linear viscous damping parameter, $k_3 =$ cubic stiffness parameter added intentionally, $c_3 =$ cubic damping parameter added intentionally.

In order to produce a dimensionless form, let

$y =$ displacement of the harmonic ground excitation

$Y =$ displacement amplitude of the harmonic ground excitation

$x^* = \frac{x}{Y}$ as the normalized absolute oscillator displacement

$z^* = \frac{x-y}{Y}$ as the normalized relative oscillator displacement

$y^* = \frac{y}{Y}$ as the normalized ground displacement

$t^* = \omega_1 t$ as the normalized time

We also define

$$\omega_1^2 = \frac{k_1}{m} \qquad \omega_3^2 = \frac{k_3}{m}Y^2 \qquad \zeta_1 = \frac{c_1}{2m\omega_1} \qquad \zeta_3 = \frac{c_3}{2m\omega_1}(\omega_1 Y)^2$$

It should be noticed that here ω_3 can be an imaginary number.

Then the cubic terms can be characterized by the dimensionless characteristic parameters p and q as:

$$p = \frac{\omega_3^2}{\omega_1^2} \qquad q = \zeta_3 \tag{2}$$

where p is a measure of the relative magnitude of the cubic stiffness nonlinearity to the linear stiffness for a specified ground motion, and q specifies the contribution of the cubic damping for a specified ground motion.

Equation (1) can be rewritten as

$$\frac{\mathrm{d}^2 z^*}{\mathrm{d}t^{*2}} + 2\zeta_1 \frac{\mathrm{d}z^*}{\mathrm{d}t^*} + z^* = -\frac{\mathrm{d}^2 y^*}{\mathrm{d}t^{*2}} + f\left(z^*, \frac{\mathrm{d}z^*}{\mathrm{d}t^*}\right) \tag{3}$$

where

$$f\left(z^*, \frac{\mathrm{d}z^*}{\mathrm{d}t^*}\right) = -2q\left(\frac{\mathrm{d}z^*}{\mathrm{d}t^*}\right)^3 - pz^{*3}$$

Next we use the Krylov-Bogoliubov 'averaging method' [16, 20–22] to obtain the approximate FRF in closed form. The harmonic ground excitation is assumed as:

$$y = Y \sin(rt^*) \tag{4}$$

where $r = \omega/\omega_1$ with ω representing the frequency of the input sinusoidal ground motion.

Thus, the solution to Equation (3) is considered to be

$$z^* = A(t^*) \sin(rt^* + \beta(t^*)) \tag{5}$$

where $A(\cdot)$ and $\beta(\cdot)$ are 'slowly varying', i.e. $A'(\cdot)$ and $\beta'(\cdot)$ are 'small', where the prime symbol represents a derivative with respect to the function argument.

If we define $\varphi = rt^* + \beta(t^*)$, then,

$$\mathrm{d}z^*/\mathrm{d}t^* = A(t^*) r \cos\varphi \tag{6}$$

Equations (4) and (6) imply,

$$A'(t^*) \sin\varphi + A(t^*)\beta'(t^*) \cos\varphi = 0 \tag{7}$$

From Equations (3), (4) and (6), we can easily obtain,

$$A' r \cos\varphi - A\beta' r \sin\varphi - Ar^2 \sin\varphi + 2\zeta_1 Ar \cos\varphi + A \sin\varphi = r^2 \sin rt^* + f \tag{8}$$

where $f(z^*, \mathrm{d}z^*/\mathrm{d}t^*)$ after substituting Equations (4) and (6) is

$$f(z^*, \mathrm{d}z^*/\mathrm{d}t^*) = -2qA^3 r^3 \cos^3\varphi - pA^3 \sin^3\varphi$$

The solutions of Equations (7) and (8) for A' and β' are

$$A' r = \cos\varphi[A(r^2 - 1)\sin\varphi + r^2 \sin(\varphi - \beta) - 2\zeta_1 Ar \cos\varphi + f] \tag{9}$$

and

$$A\beta' r = -\sin\varphi[A(r^2 - 1)\sin\varphi + r^2 \sin(\varphi - \beta) - 2\zeta_1 Ar \cos\varphi + f] \tag{10}$$

Since A and β are slowly time varying, after averaging both sides of Equations (9) and (10) over the period 2π in φ, we obtain

$$2\pi A' r = -2\zeta_1 Ar\pi - r^2 \pi \sin\beta + \int_0^{2\pi} [f(z^*, \mathrm{d}z^*/\mathrm{d}t^*) \cos\varphi]\, \mathrm{d}\varphi \tag{11}$$

and

$$2\pi A\beta' r = -A(r^2-1)\pi - r^2\pi\cos\beta - \int_0^{2\pi}[f(z^*, \mathrm{d}z^*/\mathrm{d}t^*)\sin\varphi]\,\mathrm{d}\varphi \tag{12}$$

Since we are interested in the steady-state response, the left-hand side of Equations (11) and (12) should be zero. Then after some simple calculation we have

$$r^2\sin\beta = -2\zeta_1 Ar - 1.5A^3 qr^3 \tag{13}$$

$$r^2\cos\beta = -Ar^2 + A + 0.75A^3 p \tag{14}$$

Squaring and summing Equations (13) and (14), after expansion we obtain the frequency response function of the normalized relative oscillator displacement z^*, which can be expressed as

$$(9/4)q^2A^6r^6 + (6\zeta_1 A^4 q + A^2 - 1)r^4 + (-1.5A^4 p + 4\zeta_1^2 A^2 - 2A^2)r^2 + (9/16)p^2A^6 + A^2 + 1.5A^4 p = 0 \tag{15}$$

Notice that Equation (15) is an implicit relation between r (i.e. ω/ω_1) and A.

Based on Equations (4) and (6), the FRF of the normalized absolute acceleration of the nonlinear oscillator can be easily determined as follows:

$$\mathrm{d}^2x^*/\mathrm{d}t^{*2} = -Ar^2\sin(rt^* + \beta) - r^2\sin(rt^*) \tag{16}$$

where from Equations (13) and (14),

$$\cos\beta = \frac{-r^2 + 1 + 0.75A^2 p}{\sqrt{(-2\zeta_1 r - 1.5A^2 qr^3)^2 + (-r^2 + 1 + 0.75A^2 p)^2}} \tag{17}$$

If we assume that

$$\tan\gamma = \frac{A\sin\beta}{A\cos\beta + 1}$$

then

$$\mathrm{d}^2x^*/\mathrm{d}t^{*2} = -r^2\sqrt{A^2 + 1 + 2A\cos\beta}\,\sin(rt^* + \gamma) \tag{18}$$

Distortion of the FRFs for nonlinear systems is well known. Figure 3 illustrates the effect of varying the parameter p on the shape of the FRFs. It is clear that the resonant peak moves to the left when p is a negative number, which corresponds to a softening spring and the resonant peak moves to the right for positive values of p, which corresponds to a hardening spring. The motivation to move the resonant peak to the left is to force it further from the dominant frequencies of strong ground motions. However, a very soft spring can lead to jump resonance that is undesirable (e.g. the dashed line in Figure 3). Meanwhile, a positive value of q enhances the dissipative characteristics of the controller. Optimizing p and q in order to skew the resonant peak to the left, without manifesting the jump phenomenon, results in the parameters: $p = -0.0005$, and $q = 0.00001$, where the linear damping ratio is 3% (i.e. the original linear damping characteristics are not changed). This oscillator can reduce the steady-state response (especially absolute acceleration) near the resonant frequency while keeping the response in the high frequency range ($\omega/\omega_1 > 1.4$) almost unchanged. In addition, the distorted resonant frequency of this optimal nonlinear oscillator shifts to 0.3 Hz without changing the linear

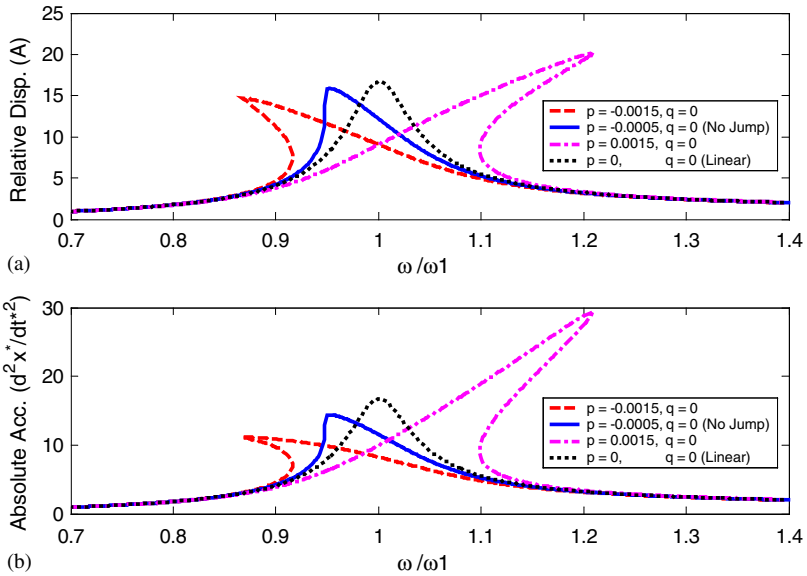

Figure 3. (a) FRFs of the normalized relative displacement with different cubic stiffness parameters; and (b) FRFs of the normalized absolute acceleration with different cubic stiffness parameters.

stiffness. This is slightly farther away from the dominant frequency of most near-fault earthquakes than the uncontrolled system.

After selecting the dimensionless characteristic parameters p and q, we can then determine the controller parameters k_3 and c_3 from Equation (2) as:

$$k_3 = \frac{m\omega_1^2 p}{Y^2} \qquad c_3 = \frac{2mq}{\omega_1 Y^2} \tag{19}$$

It should be emphasized that these parameters are dependent on the peak displacement of the harmonic ground excitation. Thus here we treat the stochastic earthquake input within the most intensive time window as a single sinusoidal excitation at its dominant frequency within the range 1–5 Hz so as to select an 'effective' peak ground displacement (PGD) from the averaged peak ground acceleration (average PGA $= 0.58g$) of all the seven benchmark earthquakes. Simulation results suggest that the value 0.014 m for the PGD (corresponding to its dominant frequency as 3.2 Hz) is most effective.

In addition, to guarantee that the 'optimal' nonlinear closed-loop system is globally asymptotically stable in the sense of Lyapunov, it is sufficient to saturate the cubic stiffness control force to keep the slope of the total restoring force ($k_1 x + k_3 x^3$) non-negative at all times as shown in Figure 4. Figure 4(a) illustrates the force generated by the linear structural stiffness, Figure 4(b) illustrates the truncated softening spring force (generated by the controller) where the truncation is used to guarantee that the slope of the total restoring force is non-negative as illustrated in Figure 4(c). The saturation value of the displacement for the optimal controller is

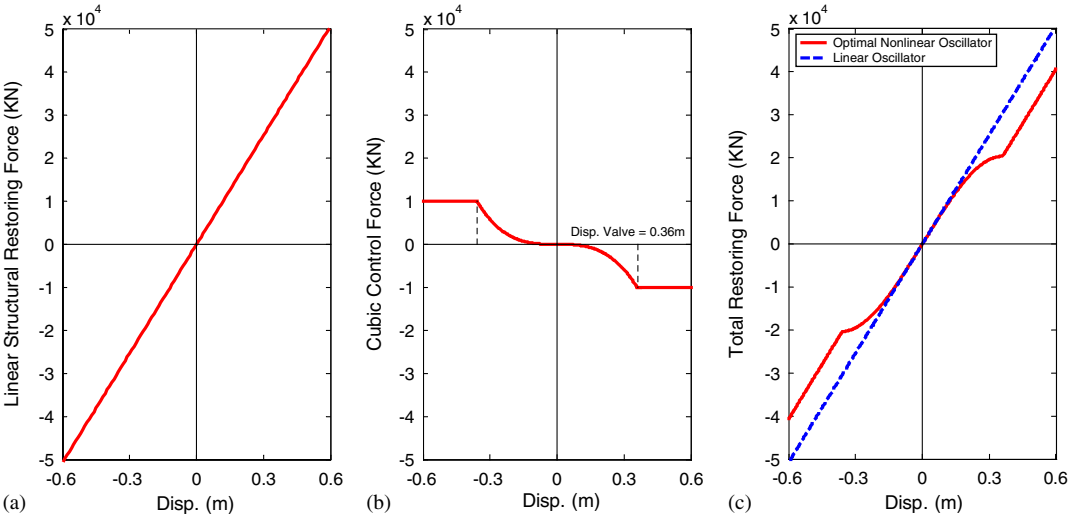

Figure 4. Force–displacement characteristics of the optimal nonlinear oscillator: (a) original linear stiffness restoring force; (b) saturation of the cubic stiffness control force; and (c) the total restoring force experienced by the structural system.

determined to be 0.36 m. Since the cubic damping parameter is selected to be positive, it will not cause any stability problem.

After obtaining the total control force at the CM of the base, we distribute it equally to the eight control devices (actuators) in each x- and y-direction as defined in the benchmark study and also as sketched in Figure 1.

3. DESIGN OF THE SEMIACTIVE CONTROLLER (SAVFD)

This section will describe a semiactive controller that endeavors to track both the aforementioned cubic active controller and the benchmark LQG active controller defined in [13], using variable viscous fluid dampers (SAVFD). This will serve to compare with the proposed cubic active control determined in the last section.

To trace a specified active control command at each sampling time for any type of semi-active damper (such as fluid viscous dampers, MR dampers, and piezoelectric friction dampers) appears to be a simple yet very effective idea [23]. Hrovat *et al.* [24] first applied this smart control algorithm to the field of structural engineering. Symans and Constantinou [25] did some shaking table tests of a controlled multi-storey scale model building subjected to seismic excitation using this Hrovat trace algorithm. Kurata *et al.* [26] installed this type of hydraulic damper in an actual building and carried out a forced vibration test. It is clear that the trace algorithm is easily realized by viscous fluid dampers. The controller output voltage (0–10 V) for each semi-active damper can be designed to be linearly dependent on the required damping

coefficient between the upper and lower bounds at each time instant in order to trace a specified active control command.

The trace algorithm is given as in [25]:

$$c_i(t) = \begin{cases} c_{\min,i} & c_i^*(t) \leqslant c_{\min,i} \\ c_i^*(t) & c_{\min,i} < c_i^*(t) < c_{\max,i} \\ c_{\max,i} & c_i^*(t) \geqslant c_{\max,i} \end{cases} \tag{20}$$

where

$$c_i^*(t) = \frac{u_i(t)}{v_i(t)} \qquad i = 1, 2, \ldots, m$$

and $u_i(t) =$ specified command for each damper regulated by the active controller, $v_i(t) =$ instantaneous velocity across each damper, $c_{\max,i} =$ maximum damping coefficient for each damper, $c_{\min,i} =$ minimum damping coefficient for each damper.

In this study, we select the maximum damping coefficient to be 3000 kN s/m for each damper so as to trace the control command well and also to allow implemention with the existing hardware. The minimum damping coefficient is set to $c_{\min} = 1/20 \times c_{\max}$ following [27]. If all the smart dampers are set to the passive-on state, we obtain a corresponding passive energy dissipation system (Passive) with about 30% linear damping of critical in the linear elastomeric isolation system.

Our simulation results show that the SAVFD control system cannot trace the cubic active controller very well in most test cases and thus will cause some performance degradation. However, the algorithm can always trace the benchmark LQG controller. Consequently, in the remainder of this paper, we show only the results for the LQG-based SAVFD system.

4. SENSOR SELECTION FOR CONTROL IMPLEMENTATION

For the cubic control system, the controller needs both the relative velocity and displacement outputs at the CM of the base. For simplicity and accuracy, the velocity and the displacement outputs at the CM of the base are represented by the actuators located at node 45 as shown in Figure 1, which is very close to the CM of the base. So, for the cubic control system, the measurements are the acceleration and displacement of the aforementioned actuators, and the ground accelerations, in the x- and y-directions. The relative velocity outputs can be determined by passing the measured accelerations through an integrator. For displacement outputs, to avoid the twice integration constant error, we directly use the measured displacements of the actuators located at node 45 near the CM and then pass them through a low-pass filter, to estimate the signals in the presence of noise. The displacement sensor gain is selected to be $10\,\text{V}/0.5\,\text{m} = 20\,\text{V/m}$, which corresponds to a peak measurable displacement of 0.5 m and a peak voltage of 10 V. Simulation results show that all the estimated signals are very close to the real values and are also very smooth, except that the estimated velocities deviate slightly from the real values at later times due to the integration constant error.

For the semi-active control system, besides the accelerations of the eighth floor, the base and the ground as in the benchmark active LQG control [13], the acceleration measurements of the 16 dampers are needed to better estimate the velocities across each semiactive viscous fluid

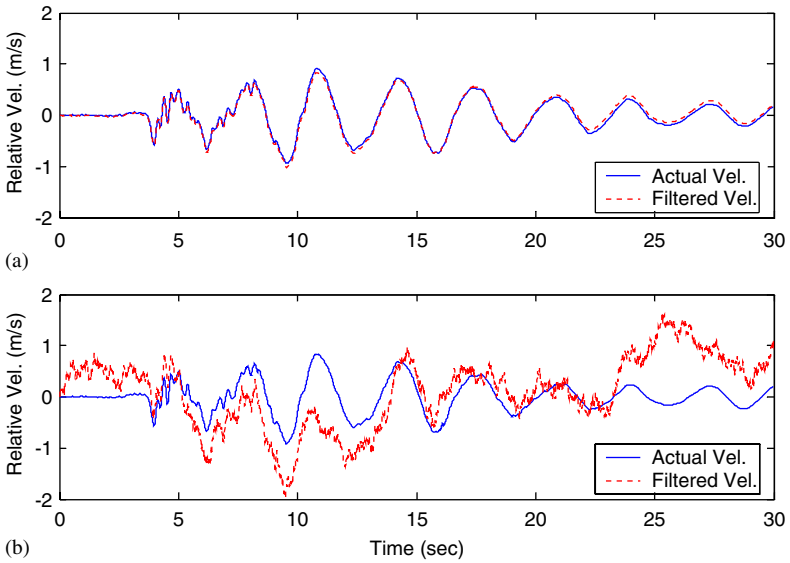

Figure 5. Comparison of the actual and estimated velocity (x-direction) of the damper located at node 3 for SAVFD under the Newhall earthquake (FP-x and FN-y): (a) our proposed sensor model; and (b) the same sensor model as in the benchmark LQG controller without acceleration sensors for each damper.

damper. From Figure 5 we can see that the addition of these sensors at each damper location can estimate the velocity of a corner damper much better than only with the measured accelerations at the CM of the base.

5. SIMULATION RESULTS AND COMPARISONS

The results of the control effect for the Cubic and SAVFD systems are presented in Tables I and II. In addition, the passive control case is added for comparison purposes. This latter case can be easily obtained by setting the smart dampers to the passive-on state. Again, for the present configuration, this provides a linear damping ratio of approximately 30%. In the tables, normalization is performed with respect to the uncontrolled base isolated building, as defined in the Appendix. Time-history responses in the NS direction for the Sylmar earthquake FP-x and FN-y components acting on the building are shown in Figure 6. The force–displacement profiles for the three control systems are also shown in Figure 7.

In the Cubic active control strategy, most of the response quantities are reduced substantially from the uncontrolled cases. The benefit of the Cubic strategy is the significant reduction of the peak and RMS floor accelerations up to 20 and 30%, respectively as well as the reduction of the peak inter-storey drifts up to 20%. It produces the smallest peak floor acceleration and peak inter-storey drift among the three proposed control strategies in most earthquakes studied here. All the peak/RMS floor accelerations and peak inter-storey drifts produced by the Cubic system

Table I. Results for Cubic, SAVFD and passive control (FP-x and FN-y).

	Case	J_1	J_2	J_3	J_4	J_5	J_6	J_7	J_8	J_9
	Cubic	0.90	0.89	0.99	0.85	0.94	0.32	0.80	0.89	0.46
Newhall	SAVFD	0.87	0.88	0.76	0.89	0.91	0.12	0.63	0.80	0.50
	Passive	0.89	1.01	0.49	1.33	1.31	0.61	0.25	0.82	0.88
	Cubic	0.68	0.70	0.81	0.78	0.83	0.33	0.58	0.61	0.53
Sylmar	SAVFD	0.91	0.94	0.90	0.91	0.95	0.12	0.60	0.80	0.54
	Passive	0.81	0.87	0.52	0.84	1.36	0.62	0.31	0.63	0.89
	Cubic	0.94	0.92	0.87	0.80	0.82	0.12	0.84	0.81	0.15
El Centro	SAVFD	0.97	0.94	0.76	0.81	0.82	0.10	0.69	0.68	0.48
	Passive	0.80	0.83	0.29	0.68	1.13	0.61	0.18	0.51	0.88
	Cubic	0.89	0.91	0.78	0.96	1.08	0.30	0.58	0.58	0.51
Rinaldi	SAVFD	0.97	0.97	0.90	0.95	0.95	0.12	0.68	0.72	0.52
	Passive	1.22	1.22	0.51	1.23	1.37	0.59	0.25	0.62	0.89
	Cubic	0.73	0.73	0.89	0.74	0.93	0.25	0.76	0.63	0.34
Kobe	SAVFD	0.82	0.83	0.73	0.83	0.91	0.12	0.68	0.69	0.50
	Passive	0.75	0.77	0.33	1.29	2.04	0.72	0.18	0.76	0.87
	Cubic	0.89	0.90	0.93	0.93	0.96	0.20	0.73	0.73	0.39
Jiji	SAVFD	0.88	0.89	0.81	0.89	0.89	0.09	0.70	0.80	0.43
	Passive	0.65	0.66	0.49	0.68	0.71	0.43	0.33	0.52	0.72
	Cubic	0.66	0.67	0.65	0.71	0.76	0.33	0.54	0.58	0.48
Erzinkan	SAVFD	0.95	0.98	0.70	0.83	0.99	0.10	0.70	0.75	0.53
	Passive	0.77	0.79	0.35	0.84	0.97	0.59	0.23	0.43	0.89

are also much smaller than those of the benchmark clipped optimal and skyhook control schemes. The base shears are also reduced up to 20% in average. These results are in good agreement with the derived nonlinear frequency response functions. Therefore this control strategy appears suitable for protecting both the superstructure and nonstructural contents in a critical base-isolated building. In addition, it is worth noting from Figure 6 that the phase of the time-history response of the Cubic system is shifted slightly from that of the uncontrolled system while the phases of the time history response of the SAVFD and passive control systems remain the same as that of the uncontrolled one. Finally, from the force–displacement profile (Figure 7a), we can see that the actuator of the Cubic control system mainly yields large II/IV quadrant forces so that the smart dampers cannot trace this behaviour very well due to their intrinsic actuating limitations. Our simulation results also verify this conclusion.

The advantage of the SAVFD semiactive control is evident in reductions of all the performance indices since it can always trace the benchmark LQG active controller very well as illustrated in Figure 8, and thus it has almost the same control effect as its active control counterpart. Consequently, for engineering application this smart system, that only relies on a few batteries, could replace the active LQG control system.

Table II. Results for Cubic, SAVFD and passive control (FN-x and FP-y).

	Case	J_1	J_2	J_3	J_4	J_5	J_6	J_7	J_8	J_9
Newhall	Cubic	0.81	0.81	1.03	0.89	0.93	0.32	1.15	0.88	0.44
	SAVFD	0.84	0.90	0.75	0.95	0.97	0.16	0.68	0.76	0.51
	Passive	0.81	0.88	0.49	1.34	1.53	0.58	0.33	0.83	0.87
Sylmar	Cubic	0.57	0.58	0.73	0.63	0.73	0.35	0.58	0.49	0.54
	SAVFD	0.90	0.89	0.88	0.89	0.92	0.13	0.67	0.69	0.57
	Passive	0.69	0.73	0.53	0.88	1.09	0.65	0.33	0.46	0.89
El Centro	Cubic	0.94	0.95	0.87	0.95	0.95	0.11	0.88	0.86	0.12
	SAVFD	0.97	0.97	0.83	0.97	1.00	0.10	0.73	0.72	0.48
	Passive	0.79	0.77	0.44	0.99	1.40	0.59	0.24	0.66	0.88
Rinaldi	Cubic	0.82	0.87	0.74	0.96	1.06	0.30	0.54	0.47	0.50
	SAVFD	0.90	0.95	0.72	0.96	0.95	0.11	0.61	0.60	0.53
	Passive	1.12	1.16	0.52	1.23	1.39	0.57	0.24	0.45	0.88
Kobe	Cubic	0.88	0.89	0.86	0.91	0.93	0.17	0.80	0.77	0.30
	SAVFD	0.98	0.98	0.77	0.98	0.96	0.11	0.76	0.78	0.42
	Passive	0.89	0.88	0.35	1.31	1.60	0.73	0.22	1.01	0.87
Jiji	Cubic	0.77	0.77	0.95	0.77	0.79	0.20	0.71	0.58	0.44
	SAVFD	0.83	0.83	0.77	0.84	0.86	0.11	0.71	0.72	0.46
	Passive	0.71	0.71	0.70	0.70	0.72	0.19	0.60	0.56	0.60
Erzinkan	Cubic	0.57	0.58	0.55	0.61	0.63	0.33	0.54	0.45	0.51
	SAVFD	0.89	0.88	0.69	0.88	0.92	0.11	0.68	0.67	0.55
	Passive	0.58	0.58	0.46	0.58	0.61	0.42	0.32	0.43	0.72

The highly damped passive energy dissipation system with 30% damping ratio in the linear isolation system reduces the peak and RMS base displacements most significantly; however, the reductions are achieved at the cost of increasing the peak/RMS floor accelerations and the peak inter-storey drifts. These results also agree with the common knowledge [28] that the heavily damped passive system may increase accelerations for flexible structures, thus highly damped passive systems may not be optimal.

6. CONCLUSIONS AND FUTURE WORK

Our study demonstrates that the Cubic active control system developed for a very flexible structure has better superstructure and nonstructural performance of absolute floor accelerations (especially if the peak evaluation criterion is considered), when compared with the SAVFD and passive systems for most test cases. Meanwhile, the Cubic system still maintains good structural performance of shears and base deformation. Therefore the proposed nonlinear feedback control system is suitable for protecting the superstructure and the nonstructural contents of a critical base isolated structure under strong near-fault earthquakes. The control effects are achieved by adding only cubic nonlinearities as a 'fine adjustment' mechanism. For

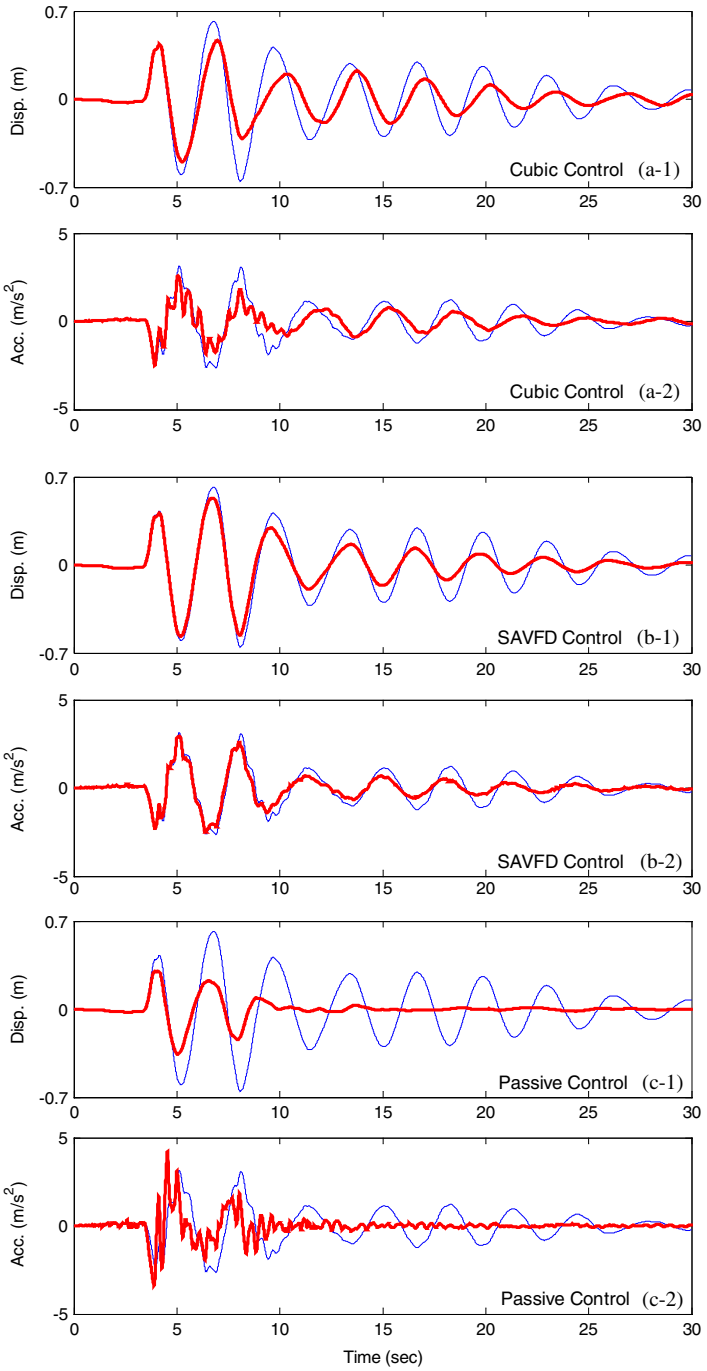

Figure 6. Time-history responses of the base displacement and top floor acceleration, for both uncontrolled (thin lines) and controlled (thick lines), at the CM of the base in the *y*-direction for Sylmar earthquake (FP-*x* and FN-*y*): (a-1,a-2) Cubic control; (b-1,b-2) SAVFD control; (c-1,c-2) Passive control.

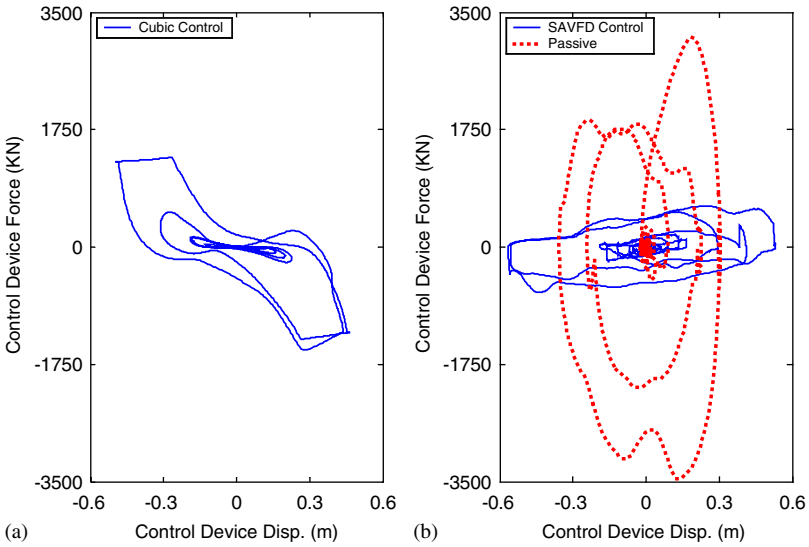

Figure 7. Force–displacement (y-direction) for Sylmar earthquake (FP-x and FN-y) and the control device located at node 45: (a) Cubic control—actuator; and (b) SAVFD and Passive control—viscous fluid damper.

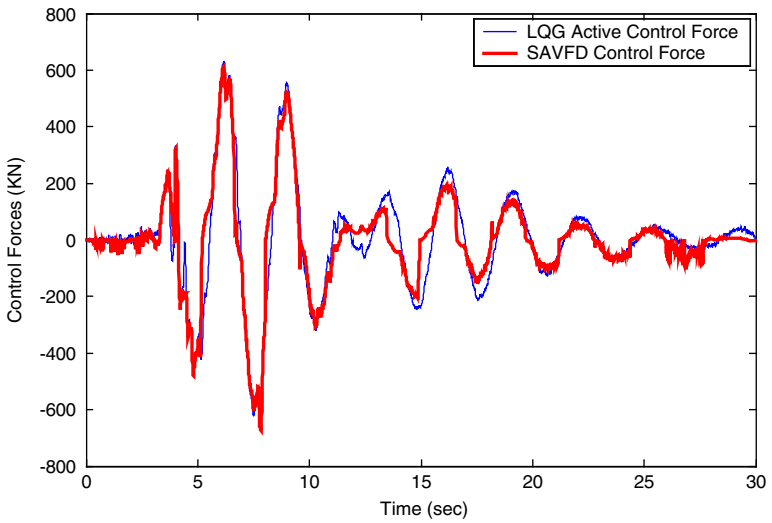

Figure 8. Comparison of the control forces (y-direction) regulated by the benchmark LQG control and the SAVFD control. Sylmar earthquake (FP-x and FN-y) and the control device located at node 45.

the SAVFD system, simulations suggest that it can trace the benchmark LQG active controller very well and thus it has almost the same control effect as its active control counterpart. Finally, results verify that heavy passive damping augmentation at the isolation level is not optimal when considering the nonstructural performance.

Obviously the optimization of the Cubic control system containing other nonlinearities, such as the phase II base isolated benchmark building with friction pendulum bearings or lead–rubber bearings, merits further study. Finally it is found that the better the estimates of the outputs, the better the performances of the Cubic control system. There is therefore motivation to study advanced filtering techniques for estimation of states.

APPENDIX

The evaluation criteria for comparing the performance of various controllers were presented by Narasimhan *et al.* [14]. These are reproduced here to assist the reader in comprehending this paper.

1. Peak base shear (isolation level) in the controlled structure normalized by the corresponding shear in the uncontrolled structure

$$J_1(q) = \frac{\max_t \| V_0(t,q) \|}{\max_t \| \hat{V}_0(t,q) \|}$$

2. Peak structure shear (at first storey level) in the controlled structure normalized by the corresponding shear in the uncontrolled structure

$$J_2(q) = \frac{\max_t \| V_1(t,q) \|}{\max_t \| \hat{V}_1(t,q) \|}$$

3. Peak base displacement or isolator deformation in the controlled structure normalized by the corresponding displacement in the uncontrolled structure

$$J_3(q) = \frac{\max_{t,i} \| d_i(t,q) \|}{\max_{t,i} \| \hat{d}_i(t,q) \|}$$

4. Peak inter-storey drift in the controlled structure normalized by the corresponding inter-storey drift in the uncontrolled structure

$$J_4(q) = \frac{\max_{t,f} \| d_f(t,q) \|}{\max_{t,f} \| \hat{d}_f(t,q) \|}$$

5. Peak absolute floor acceleration in the controlled structure normalized by the corresponding acceleration in the uncontrolled structure

$$J_5(q) = \frac{\max_{t,f} \| a_f(t,q) \|}{\max_{t,f} \| \hat{a}_f(t,q) \|}$$

6. Peak force generated by all control devices normalized by the peak base shear in the controlled structure

$$J_6(q) = \frac{\max_t \left\| \sum_k F_k(t,q) \right\|}{\max_t \| V_0(t,q) \|}$$

7. RMS base displacement in the controlled structure normalized by the corresponding RMS base displacement in the uncontrolled structure

$$J_7(q) = \frac{\max_f \|\sigma_d(t,q)\|}{\max_f \|\sigma_{\hat{d}}(t,q)\|}$$

8. RMS absolute floor acceleration in the controlled structure normalized by the corresponding RMS acceleration in the uncontrolled structure

$$J_8(q) = \frac{\max_f \|\sigma_a(t,q)\|}{\max_f \|\sigma_{\hat{a}}(t,q)\|}$$

9. Total energy absorbed by all control devices normalized by energy input into the controlled structure

$$J_9(q) = \frac{\sum_k \left[\int_0^{T_q} F_k(t,q) v_k(t,q)\,\mathrm{d}t\right]}{\int_0^{T_q} \langle V_0(t,q)\ddot{U}_g(t,q)\rangle\,\mathrm{d}t}$$

where, i = isolator number, $1,\ldots,N_i$ ($N_i = 8$); k = device number, $1,\ldots,N_d$; f = floor number, $1,\ldots,N_f$; q = earthquake number: $1,\ldots,5$; t = time, $0 \leqslant t \leqslant T_q$; $\langle\bullet\rangle$ = inner product; $\square\bullet\square$ = vector magnitude incorporating NS and EW components.

ACKNOWLEDGEMENTS

Partial funding provided by the Earthquake Engineering Research Centers Program of the US National Science Foundation under NSF Award Number EEC-9701471 is gratefully acknowledged. Any opinions, findings and conclusions or recommendations expressed are those of the authors and do not necessarily reflect those of the National Science Foundation. Additionally, the authors would like to thank Professor T. T. Soong, State University of New York at Buffalo for his valuable suggestions.

REFERENCES

1. Villaverde R. Nonlinear seismic response of nonstructural elements attached to buildings. *Technical Report*, Department of Civil Engineering, University of California, Irvine, 1986.
2. Soong TT, Dargush GF. *Passive Energy Dissipation Systems in Structural Engineering*. Wiley: New York, 1997.
3. Gavin H, Aldemir U. Behavior and response of auto-adaptive seismic isolation. *Proceedings of the 3rd U.S.—Japan Workshop in Urban Earthquake Disaster Mitigation*, Seattle, WA, 15–16 August, 2001; 120–128.
4. Inaudi JA, Kelly JM. Optimum damping in linear isolation systems. *Earthquake Engineering and Structural Dynamics* 1993; **22**:583–598.
5. Beck JL, Yuen KV. Stochastic approach to control and identification of smart structures. *Proceedings of the International Conference on Advances in Building Technology*, Hong Kong, China, 2002; 457–464.
6. Housner GW, Bergman LA, Caughey TK, Cassiakos AG, Claus RO, Masri SF, Skelton RE, Soong TT, Spencer BF, Yao JTP. Structural control: past, present and future. *Journal of Engineering Mechanics* (ASCE) 1997; **123**(9):897–971.
7. Iwan WD, Wang LJ. New developments in active interaction control. *Proceedings of the 2nd International Workshop on Structural Control*, Hong Kong, China, 1996.
8. Soong TT. *Active Structural Control*: *Theory and Practice*. Longman: New York, 1990.
9. Spencer BF, Dyke SJ, Sain MK, Calson JD. Phenomenological model of a magnetorheological damper. *Journal of Engineering Mechanics* (ASCE) 1997; **123**(3):230–238.

10. Spencer BF, Johnson EA, Ramallo JC. Smart isolation for seismic control. *JSME International Journal*, *Series C* 2000; **43**(3):704–711.
11. Yang J, Agrawal A. Semiactive hybrid control systems for nonlinear buildings against near-field earthquakes. *Journal of Engineering Structure* 2002; **24**:271–280.
12. Nagarajaiah S, Narasimhan S. Phase I: controllers for benchmark base isolated building: Part I. *Proceedings of the 4th International Workshop on Structural Control and Health Monitoring*, Columbia University, 10–11 June 2004.
13. Nagarajaiah S, Narasimhan S. Smart base-isolated benchmark building part II: sample controllers for linear isolation system. *Journal of Structural Control and Health Monitoring* 2006.
14. Narasimhan S, Nagarajaiah S, Johnson EA, Gavin HP. Smart base-isolated benchmark building part I: problem definition. *Journal of Structural Control and Health Monitoring* 2006.
15. Jackson EA. *Perspectives of Nonlinear Dynamics*. Cambridge University Press: Cambridge, UK, 1989.
16. Stoker JJ. *Nonlinear Vibrations in Mechanical and Electrical Systems*. Interscience Publishers: New York, 1950.
17. Chopra AK. *Dynamics of Structures*. Prentice-Hall: Englewood Cliffs, New Jersey, 1995.
18. Wu Z, Lin RC, Soong TT. Non-linear feedback control for improved peak response reduction. *Journal of Smart Materials and Structures* 1995; **4**:140–147.
19. Wu Z, Soong TT, Gattulli V, Lin RC. Nonlinear control algorithms for peak response reduction. *National Center for Earthquake Engineering Research Technical Report NCEER-95-004*, 1995.
20. Nakhaie JR, Narimani A, Golnaraghi MF. Practical frequency and time optimal design of passive linear vibration isolation mounts. *International Journal of Vehicle Mechanics and Mobility* (*Vehicle System Dynamics*) 2003; **39**(6):437–466.
21. Šiljak DD. *Nonlinear Systems—The Parameter Analysis and Design*. Wiley: New York, 1969.
22. Vidyasagar M. *Nonlinear Systems Analysis*. Prentice-Hall: Englewood Cliffs, New Jersey, 1993.
23. Ou J. *Structural Vibration Control*. Science Press: Beijing, China, 2003.
24. Hrovat D, Barak P, Rabins M. Semiactive versus passive or active tuned mass dampers for structural control. *Journal of Engineering Mechanics* (ASCE) 1983; **109**(3):691–705.
25. Symans MD, Constantinou MC. Seismic testing of a building structure with a semiactive fluid damper control system. *Earthquake Engineering and Structural Dynamics* 1997; **26**:759–777.
26. Kurata N, Kobori T, Takahashi M, Ishibashi T, Niwa N, Tagami J, Midorikawa H. Forced vibration test of a building with semiactive damper system. *Earthquake Engineering and Structural Dynamics* 2000; **22**:925–941.
27. Yoshida K, Yoshida S, Takeda Y. Semiactive control of base isolation using feedforward information of disturbance. *Proceedings of the 2nd World Conference on Structural Control*, Kyoto, Japan, 1998; **1**:377–386.
28. Sadek F, Mohraz B. Semiactive control algorithms for structures with variable damper. *Journal of Engineering Mechanics* (ASCE) 1998; **124**(9):961–990.

